Experimental method for dynamic residual strength characterisation of aircraft sandwich structures

N.W. Bailey[a]*, M.A. Battley[a] and M. Zhou[b]

[a]Department of Mechanical Engineering, The University of Auckland, Auckland, New Zealand; [b]The George W. Woodruff School of Mechanical Engineering, Georgia Institute of Technology, Atlanta, Georgia, USA

This study investigates the effect of dynamic loading on the residual of sandwich structures used in aircraft interiors comprising glass fibre phenolic resin face sheets and Nomex® honeycomb core. A dynamic edgewise compression test method for residual strength testing of sandwich structures has been developed using a modified compressive Split Hopkinson Pressure Bar apparatus. Dynamic edgewise compression at strain rates of approximately 50 s^{-1} for undamaged specimens showed an average increase of 26% in compression strength compared with equivalent static edgewise compression tests. For low levels of indentation damage there was a 27% reduction in residual dynamic compressive strength compared with a 15% reduction in residual static compressive strength for equivalent prior damage. This new experimental method provides insights into the dynamic edgewise response of composite sandwich structures to aid in the design and development of future aeronautical structures.

Keywords: sandwich; honeycomb; dynamic; aircraft

1. Introduction

Sandwich structures comprising thin face sheets and a cellular core have been used extensively in aerospace applications for their high strength, stiffness and associated weight savings. Due to their geometrical configuration, sandwich structures have several possible failure modes depending on the loading conditions, which include face sheet fracture, wrinkling, core shear failure, shear crimping and global buckling [11, 26]. Phenolic-based glass fibre-reinforced plastics (GFRP) are widely used in interior aircraft applications due to their superior flammability resistance. A commonly used core is phenolic-impregnated aramid fibre paper such as the product range known as Nomex® honeycomb.

Structures must meet strict design requirements that are intended to maintain their structural integrity under dynamic loading typical of an associated crash landing. Regulations specify that aircraft must be capable of withstanding significant loads, some replicating a survivable crash. Specifically, Federal Aviation Regulation Part 25, Section 25.561 on Emergency Landing Dynamic Conditions, describes the certification loads that items of mass must be certified to [7]. This states that components must be able to withstand peak floor decelerations of up to 9.0 g forward.

Classification of in-plane compression for design allowables is typically carried out using the edgewise compression method as described in ASTM C364 – 'Standard Test Method for Edgewise Compressive Strength of Sandwich Constructions' [2] or the beam flexural test method ASTM D7249 – 'Standard Test Method for Facing Properties of Sandwich Constructions by Long Beam Flexure' [1].

Thin face sheet sandwich structures loaded in compression are likely to fail by wrinkling of the face sheet [3]. This instability failure mode is governed by the critical load at which the core can no longer stabiles the face sheet which buckles locally into or out of the core. Usually this local buckling failure occurs with a very small wavelength and is immediately followed by catastrophic failure of the structure as the opposite face sheet cannot support the load. The face sheet fractures as a result of localised buckling and the failure can often be mistaken for pure compression failure of the face sheet material. Failure is attributed to wrinkling failure due to the lower critical load than what would be expected from a pure compressive failure of the face sheet material [12, 16]. Wrinkling failure can be approximated by the Hoff wrinkling approximation given in Equation (1) [14] (where E_f is the face sheet modulus, E_c is the out-of-plane core modulus and G_c is the core shear modulus). This semi-empirical failure criteria was developed based on a strain energy formulation and a series of experimental edgewise compression tests. Since 1945 this criteria has been widely used for design purposes as a conservative estimate of the critical wrinkling failure stress (σ_{cr}),

*Corresponding author. Email: nbai010@aucklanduni.ac.nz

$$\sigma_{\mathrm{cr}} = 0.5 \; \left(E_f E_c G_c \right)^{\frac{1}{3}}. \qquad (1)$$

Dynamic loading can cause additional and more complex failure modes to occur due to interacting rate-dependant material properties, inertial effects and wave propagation within the components of the sandwich structure [12, 22]. Previous studies have mainly focused on rate-dependent material classification of the constituent components used in sandwich structures. For honeycomb sandwich structures the dynamic effects may vary in the core and face sheet components due to different constituent materials and cellular geometry. A study on the separate face sheet and core constituents susceptibility to strain rate by Heimbs et al. [11] found that for a strain rate of 50 s^{-1} the tensile strength of phenolic-based GFRP increased on average by 88% compared to static loading. The reasons for this are not certain; however, one theory attributes the increased strength at higher strain rates to changes in the failure mechanisms, such as an increase in fibre matrix interface failure [4]. Heimbs also showed that the rate effect of Nomex$^{®}$ honeycomb is also significant, with an increase of 25% in stabilised out-of-plane crush strength for a strain rate of 125 s^{-1}. For in-plane compression of Nomex$^{®}$ honeycomb at 50 s^{-1}, the plateau stress increased by 33%. The rate dependency in the honeycomb is attributed to the inertial effects during local buckling and resulting permanent deformation of cell walls, rather than material rate effects [10, 27].

Experimental techniques to dynamically test materials, including metals and composites, are difficult to perform when compared with static test methods and the results are often difficult to interpret [4]. A review of dynamic testing equipment by Barré et al. [4] described the advantages of some commonly used test systems. The most popular is the Split Hopkinson Pressure Bar (SHPB) system as it offers high strain rate testing capability of up to 10^4 s^{-1} [22]. Other systems used for the testing of composites include drop weight impact test machines and shock tube systems. SHPB systems operate on the principle of detecting strain differences in measurements taken from gauges located on the incident and transmission bars to determine the impact-history of the dynamic event. Stress and strain derivations are based on the elastic bar wave theory for a pulse propagating in a uniform bar. A full description of the SHPB theory can be found in [17]. Common configurations of an SHPB system consist of a series of concentrically aligned steel rods mounted on a rigid frame that allows longitudinal movement of the rods through lubricated collars. Historically, Hopkinson pressure bar test apparatus has been widely used to evaluate high strain rate effects using a torsion bar, spring or a gas gun launch system [22]. The apparatus can be tailored for different testing modes (compression, tension and shear) to obtain data on strain rate sensitivity, dynamic yield stress, damage propagation and failure mechanisms. The SHPB is designed for medium strain rate testing with load rates typically between 10^2 s^{-1} and 10^4 s^{-1} [22].

Previous work has been carried out by others to modify the SHPB system to incorporate composite materials. Park et al. [19] used a compression SHPB apparatus to characterise the mechanical response of glass and carbon fiber-reinforced laminates to transverse impact in a three-point loading configuration. Gilat et al. [8] modified a standard SHPB to successfully incorporate a polymer matrix specimen. Mahfuz et al. [18] modified the conventional SHPB system for testing soft materials (soft core sandwich structures) by replacing the steel transmitter bar with a polycarbonate bar.

For this set of work, a compression SHPB was used as the experimental test system. A strain rate of 50 s^{-1} was selected for this test program based on the investigations by Heimbs et al. [11] into relevant loading rates for interior aircraft components manufactured from Nomex$^{®}$ honeycomb and phenolic resin-based GFRP. The advantage of using this strain rate with an SHPB system is that there is capability to increase the strain rate for future work and the results can be compared to drop weight impact tests of the same edgewise compression configuration. A test program is underway to replicate dynamic edgewise loading using a fully instrumented drop weight impact test machine. This will provide comparative results to determine the effectiveness of the modified Hopkinson bar technique developed here.

Damage tolerance for aerospace composites is generally defined as the capability of the structure to sustain an impact event and retain appropriate residual strength [22]. A major concern with sandwich structures is the susceptibility of honeycomb sandwich structures to impact damage and the potential reduction in structural integrity. In-service damage in an aircraft cabin from sources such as maintenance operations or luggage and trolley impacts has the capability to significantly reduce the load-carrying capacity of the structure [9].

Residual strength characterisation of the structure is complex because of the interactions between the face and core constituents [24]. One method to classify damage is to separate the damage into two classes depending on the severity, firstly scratches and dents, and secondly cracks/punctures, which penetrate the face sheet. The distinct difference between these types of damages is that damage that penetrates the face sheet is more likely to be observed during maintenance checks. Damage that is difficult to detect during routine visual inspections is often referred to as Barely Visible Impact Damage (BVID) and this type of damage may have a significant effect on the structural integrity of the component.

Out-of-plane indentation of sandwich structures typically results in both face sheet and core damage. In the case of thin face sheet sandwich structures, the face sheet damage radius (R_f) has been shown to be approximately
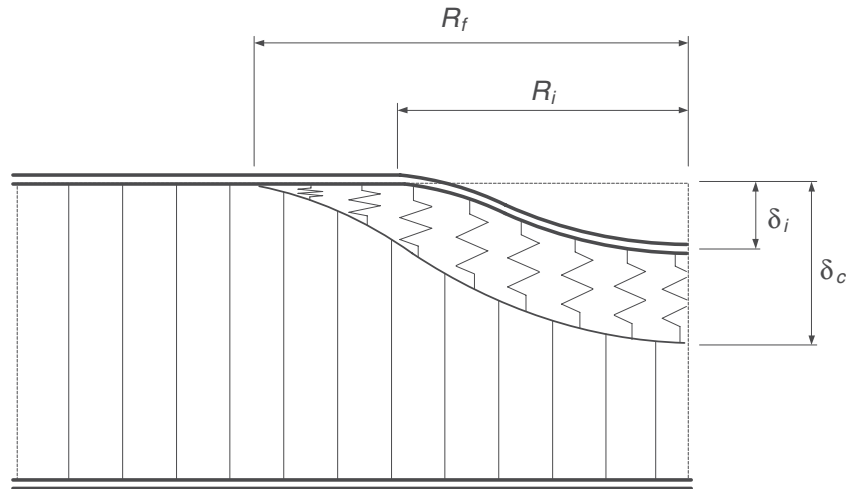
Figure 1. Damage characterisation, R_f – core damage diameter, R_i – face sheet damage diameter, δ_i – face sheet indentation, δ_c – core indentation.

equal to the crushed core radius (R_i) [21]. Residual damage depth (δ_i) is a convenient way to classify the damage for this material as the depth can be measured directly on the sample without sectioning the specimen. Honeycomb core is susceptible to core crushing due to buckling of cell walls at critical loads. The crushed core damage (δ_c) may extend below the visible indentation radius of the face sheet as shown in Figure 1. The region of face sheet damage (R_f), can include fibre breakage, matrix cracking and delamination. This damage can cause reduction in stiffness of the face sheet in this region and initiate failure during residual strength testing.

Low velocity impact to replicate the in-service damage events is typically carried out using a drop weight impact test system; however, this method can create large variations in the damage characteristics [23]. An alternative method of damage creation, quasi-static indentation, has been shown to approximate low velocity impact scenarios very well and is widely used as it enables production of consistent and repeatable damage [25]. Quasi-static indentation is also relevant for interior aircraft materials due to the mechanism of damage; large forces apply slowly but concentrate over a small area, simulating damage from high heel shoes or other passenger-related damage phenomena.

The aim of this study is to investigate how dynamic loading affects the compressive response of the sandwich structure at a coupon level for an edgewise loading configuration. Residual dynamic compressive strength is investigated in two stages: out-of-plane quasi-static indentation damage creation with a hemispherical indentor followed by dynamic edgewise compression. The work presented outlines a dynamic residual strength test method for sandwich structures, including the modification and implementation of the experimental method, calibration and validation and the results of the test program.

2. Materials and specimens

The material used for the main test program is a sandwich composite used extensively in modern aircraft interiors. This material is used to manufacture class partitions, coat lockers, overhead lockers, galleys and furniture. A standard panel thickness of 25.4 mm (1 inch) was used, comprising a Nomex® honeycomb core (HRH 10-3.0) and a glass-phenolic face sheet (Norbond L528-7781) with material properties given in Table 1. All specimens were machined to a size of 115 mm in length and 75 mm in width. Additional specimen information is provided in the schematic shown in Figure 2. The stiffer ribbon direction of the core

Table 1. Sandwich panel material properties [11, 13].

|	Face sheet glass-phenolic	Core Nomex® honeycomb 1/8-3.0
Density, ρ (kg/m³)	1600	48
Thickness, t (mm)	0.5	24.4
Longitudinal modulus, E_1 (MPa)	23,000	0.44
Transverse modulus, E_2 (MPa)	23,000	0.29
Compressive modulus (MPa)	—	138
Longitudinal shear modulus, G_{13} (MPa)	—	40
Transverse shear modulus, G_{23} (MPa)	—	25
Longitudinal strength, σ_1 (MPa)	300	—
Transverse strength σ_2 (MPa)	300	—
Compressive strength σ_3 (MPa)	—	2.3
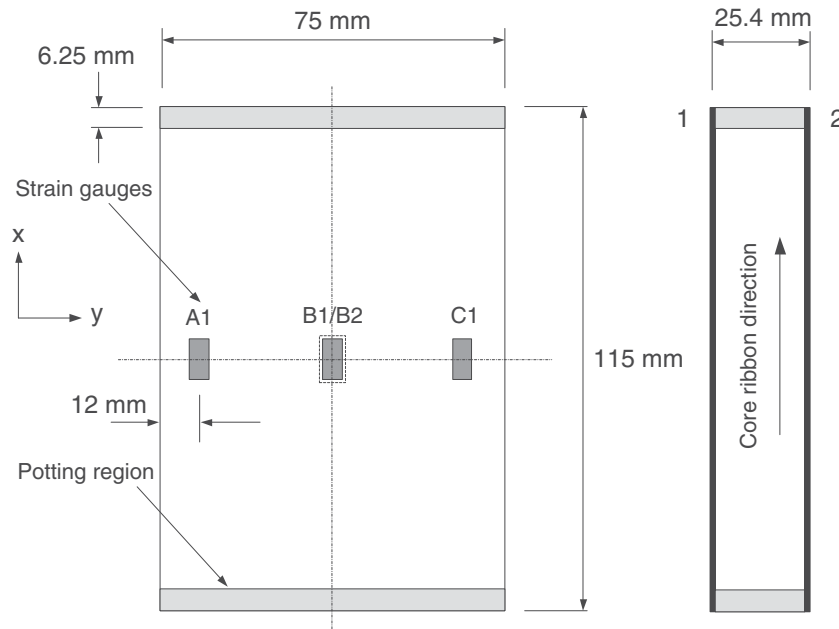
Figure 2.   Specimen geometry showing strain gauge placement and resin potting regions.

was aligned along the length of the specimen and used as the primary loading direction. Potting of the specimen ends was required to prevent premature failure of the specimens at the platen contact points. If the ends are not stablilised, the free edge of the unsupported face sheet separates from the core before failure of the sandwich structure occurs in the gauge length. Potting of the ends involved machining away the core to a depth of 6.35 mm with a standard milling machine. A compound comprising epoxy resin (West System 105) mixed with a phenolic micro-balloon filler (West System 407) was used to fill the ends of the sandwich specimens to replace the core. A flat aluminum mould was used to prepare the end surfaces of the specimens. Post-machining of the ends was also carried out to maintain the flatness and parallelism of the end surfaces to a tolerance of 0.02 mm. This step was critical to minimise possible uneven loading of face sheets, which may result in bending of the specimen causing premature failure. To ensure that the load distribution was even between the face sheets, resistance strain gauges (WK-06-250BF-10C, Gauge factor of 2.05) were attached to the face sheet surface. The schematic in Figure 2 shows where the gauges were placed; strain gauges A1 and C1 were located on the edge of the front face sheet where $Y_1 = 12$ mm, B1 and B2 were located in the centre of the front and back face sheets respectively (numbers 1 and 2 refer to the front and back face sheets). This arrangement of gauges allowed the measurement of strain distribution between the two face sheets (gauges B1 and B2) and also across the width of the face sheets (gauges A1 and C1).

3.   Experimental methods

3.1.   Damage creation

Damage creation was carried out using quasi-static indentation of a 25.4-mm diameter hemispherical indentor to induce varying degrees of out-of-plane compressive damage. The loading rate was set at a constant speed of 0.5 mm/min and the specimen was supported by a rigid platen.

Initial experiments were carried out to a depth of 6 mm to determine the damage characteristics of the sandwich structure when loaded in the out-of-plane direction. The indentor was displaced into the face sheet up to 6 mm and the force-displacement profile is shown in Figure 3. The results show a linear increase in the force response until a displacement of approximately 2.5 mm at a load of 625 N. During the linear loading phase, the local damage to the face sheet and local core crushing were the predominant damage mechanisms observed. At the maximum load point significant cracking of the face sheet starts to occur and there is a 20% average decrease in compressive load. After a displacement of approximately 2.5 mm there is a penetration of the face sheet and the failure mode shifts predominantly to core crushing. The variability in damage increases after this point as shown by the standard deviation profiles in Figure 3 (based on a sample of seven specimens).

The next phase of testing involved the classification of damage in terms of the residual dent depth. This was carried out using a loading and unloading test. The indentor was displaced into the specimen to the required depth and then removed at the same loading rate. The displaced
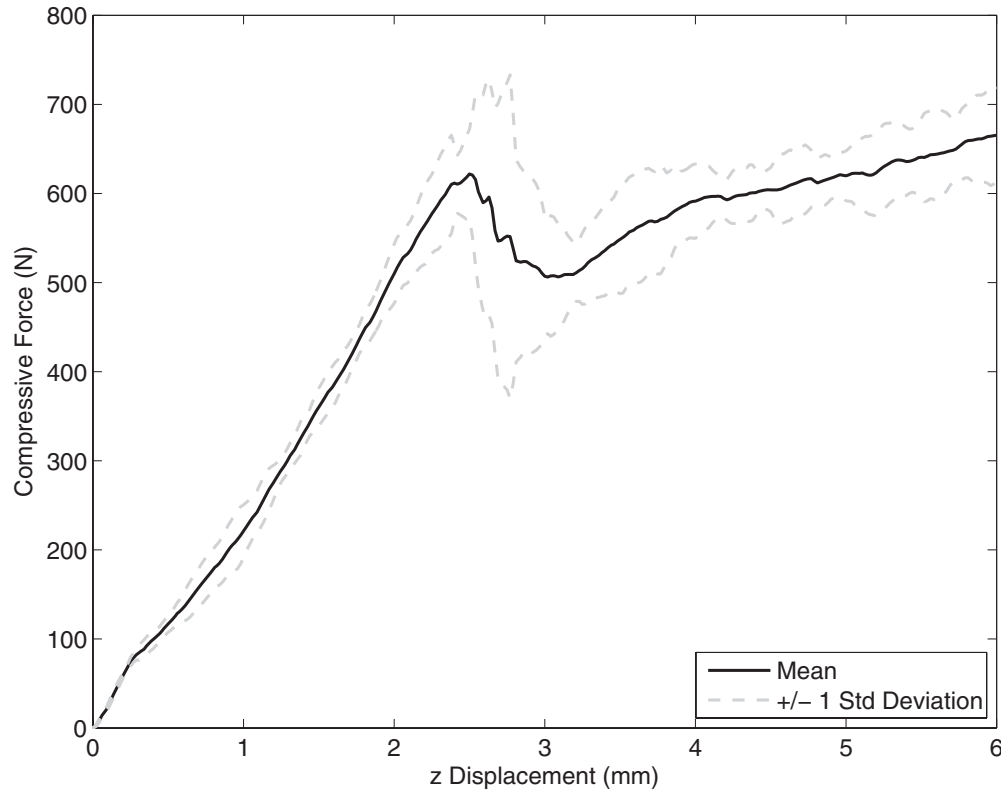
Figure 3.   Force-displacement profile for quasi-static indentation using a 25.4-mm hemispherical indentor.

depth at which the compressive load reached zero during the unloading stage was defined as the residual dent depth. This test was carried out for displaced depths of 0 to 6 mm in 1-mm increments. Results in Figure 4 show three main stages during loading: an initial loading region with a minimal variation in the damage, a step change increase in residual dent depth between 2 mm and 3 mm, and a final region with more variability in the damage created. At 2.5-mm indentation cracking and splitting of the face sheet starts to occur, hence damage depths beyond this are likely to be easily identified during routine maintenance inspections. Indentation depths of 1, 2 and 3 mm were used in this study to replicate BVID, creating damage with residual dent depths of 0.22, 0.67 and 1.7 mm respectively. The degree of damage will be referred to using these residual dent depth values.

3.2. Static edgewise compression

Static residual strength testing was carried out as per ASTM C364 [2] as a comparative study for the dynamic residual strength test method under development. Specimens were clamped using fixtures at both ends of the specimen to transfer the load evenly from the spherical loading head and to the base of the universal testing machine as shown in Figure 5. A displacement rate of 0.5 mm/min was applied,

which induced failure within the specified time range of 3–6 min for the test method. Strain gauges were used to ensure that alignment of the loading platens was uniform. Strain gauges were located in the centre of each face sheet gauges (B1 and B2 in Figure 2).

The standard defines acceptable failure modes as being those occurring within the gauge length of the specimen one thickness distance from each end of the specimen. Wrinkling failure is the most likely failure mode with the sandwich structure configuration used in this study; however, observation and verification of wrinkling failure actually occurring is difficult. An Olympus high-speed camera (i-Speed 2) was used to capture the failure of the sandwich structure at 10,000 fps. Tests were carried out with the camera orientated normal and to the face sheet. A total of nine undamaged specimens were tested and five samples of each damage depth were tested.

Compressive strength was derived based on the antiplane core assumption that no axial load is distributed to the honeycomb core in the loading direction and the face sheets share the applied load equally. The critical stress was calculated using the expression given in Equation (2), where F is the applied load, t is the face sheet thickness and W is the width of the specimen [16]:
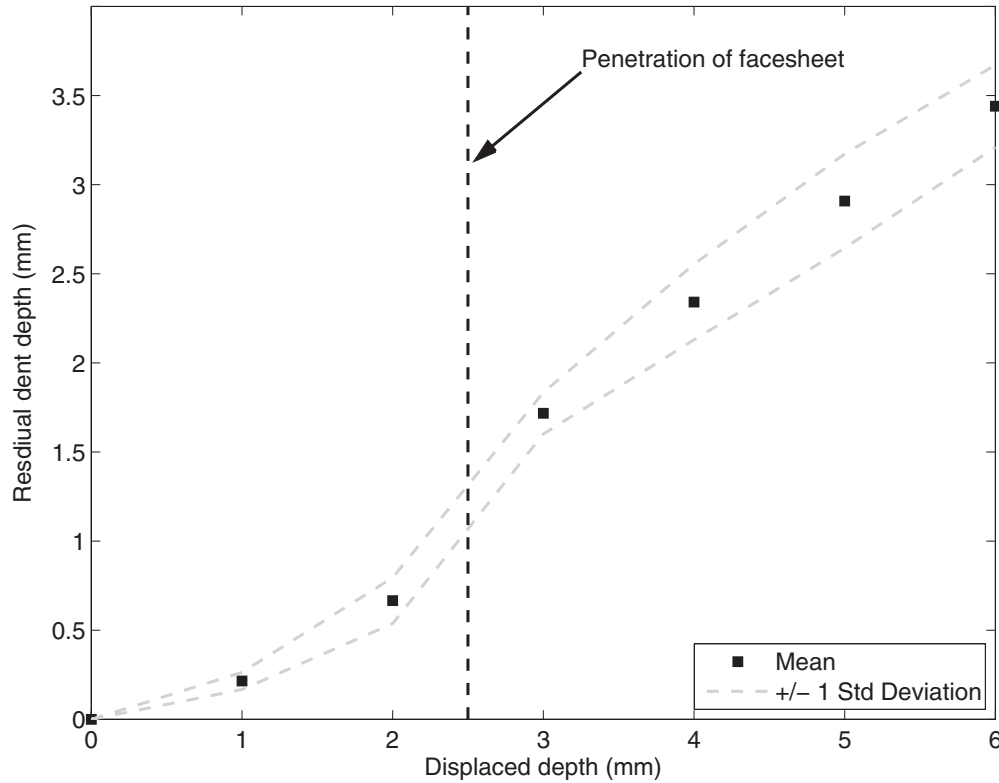
$$\sigma_{cr} = \frac{F}{2tW}. \tag{2}$$

Figure 4.   Residual dent profile for quasi-static indentation using a hemispherical indentor.

3.3.   *Dynamic edgewise compression*

The SHPB system configuration used for this study uses a gas gun to fire a projectile along the gun barrel into the incident bar as shown in Figure 6. This generates a stress wave that propagates along the incident bar through the specimen and into the transmission bar. Initial and reflected waves are recorded via strain gauges located on the incident and transmission bars at the locations indicated in Figure 6.

From the strain–time histories of incident and transmission bars, the stress (σ_s) in the specimen can be calculated using Equation (3), where E is the Young's modulus of impact bars, A_o is the cross-sectional area of impact bars and A is the cross-sectional area of the specimen face sheets. The strains, ε_i, ε_R and ε_T are recorded at the incident, reflected and transmission locations respectively. The 'reflected' location refers to the wave recorded in the incident bar after reflection from the specimen interface. This assumes that the core does not take any of the in-plane stress (antiplane core assumption) as used in the static edgewise compression method. The strain in the specimen (ε_s) is derived using the expression given in Equation (4), where c_o is the speed of sound in the bars, L is the length of the specimen and ε_R is the reflected strain recorded in the incident bar:

$$\sigma_s = \frac{EA_o}{2A}\left(\varepsilon_i + \varepsilon_R + \varepsilon_T\right), \tag{3}$$

$$\varepsilon = -2\int_0^t \frac{c_o}{L}\varepsilon_R(t)dt. \tag{4}$$

A typical specimen used for Hopkinson bar compression tests of homogeneous materials is in the order of 5–10 mm in diameter. Modification to the interface configuration (between the incident bar, specimen and transmission bar) was required to incorporate a significantly larger sandwich specimen. The focus of this modification was the distribution of the stress wave from the 19-mm circular rods of the SHPB system to the edge of the specimen. The aim was to create a planar stress wave across the full width of the specimen. Steel fixtures were designed to transfer the load across the width of the specimen using a tapered shape to minimise the size of fixtures and limit the addition of mass into the system. Explicit Finite Element Analysis (FEA) was carried out on potential modifications to the current SHPB system. Simulation of the dynamic impact was performed using Abaqus 6.9 to assist with the design of the fixture geometry. A linear elastic material model was implemented using the material properties given in Table 1. Solid elements were used for the core region (C3D8R) and shell elements for the face sheets (S4R) with a global element size of 3 mm. The fixture and incident and transmission bars were also modelled using solid elements. The model comprised approximately

N.W. Bailey et al.

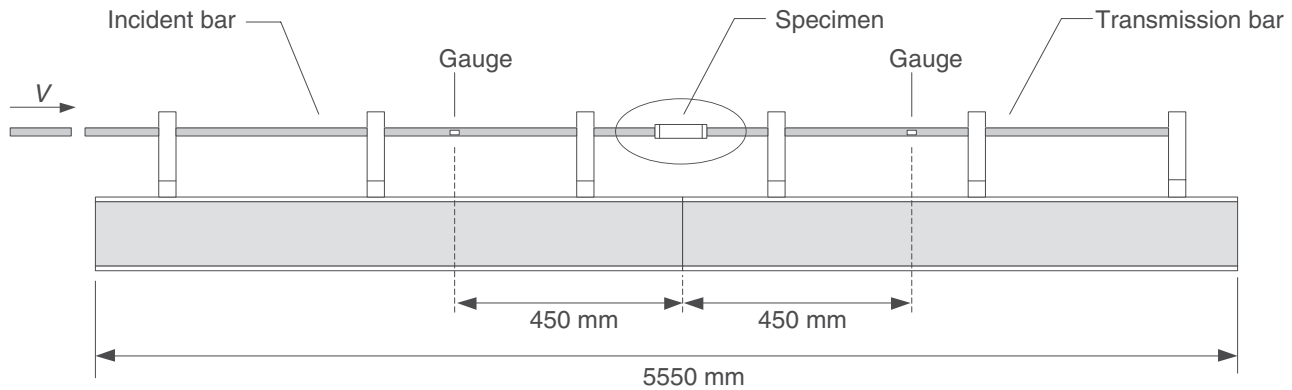Figure 5.   Configuration for static edgewise compression experimental tests.

Figure 6.   Experimental layout of Split Hopkinson Pressure Bar (SHPB).

34,000 elements for the original configuration (Figure 7a) and 50,000 elements for the modified configuration with the new fixtures attached (Figure 7b). Simulations were carried out to determine what effect the addition of the modification had on the propagation of stress waves in the specimen, with stress wave results shown in Figure 8 at 20 μs after the initial impact. The simulation modelled the impact for a total of 400 μs. Analysis of the fixture was carried out with an initial velocity of the incident bar of 5.5 m/s to replicate the desired loading strain rate of 50 s^{-1}. For the unmodified configuration, the stress results shown in Figure 8a illustrate a localized stress concentration at the impact point which develops into a narrow stress wave as it propagates through the specimen. The maximum stress in the concentrated area near the impact point observed in Figure 8a is 37% greater than the maximum stress in the same area shown in Figure 8b, demonstrating that the modification improves the dispersion of energy across the width of the specimen and increases the uniformity of loading.

The final fixture design is shown in Figure 9. The specimen slides into the middle slot but is not clamped. A recess in the angled fixture and a centering ring are used to align the fixture with a cylindrical steel bar of the test rig. The region of the specimen supported in the *z*-direction is the part of the specimen, which is lightly clamped in the static edgewise method ASTM C364 [2]. The modified SHPB test configuration with additional fixtures is shown in Figure 10.

Calibration of the SHPB system requires the transmission and incident bars to be configured without an attached specimen [2]. To calibrate, strain pulses from an impact are recorded at the incident and transmission locations and the two recorded pulses should be 'approximately identical and rectangular in shape' [2]. The SHPB was installed with new fixtures and an impact carried out. Strain profiles shown in Figure 11 show similar pulses in terms of magnitude, and the shape is rectangular as required. The first pulse shown in Figure 11 is the wave propagating through the incident bar and the second pulse is the wave that propagates through the transmission bar. The pulse recorded in the transmission bar has to pass through the interface at the boundary between the incident and transmission bars which in this test case means that the pulse also has to pass through the new fixtures attached to the end of each bar. As the strain pulses were approximately identical and rectangular in shape, it suggested that the new fixtures were adequately incorporated into the SHPB system.

Tests were carried out at various gas gun pressures to determine the relationship between set pressure, impact velocity and strain rate. For the target strain rate of 50 s^{-1} this correlated to a gas gun pressure of 40 psi, which was used for the main test program. An impact mass of 1.35 kg was used for the striker bar projectile. A high-speed camera (Imacon 200) was used to capture the impact event to evaluate damage propagation and failure in the face sheet of the sandwich specimen. The high-speed camera was orientated normal to the face sheet to capture the crack propagation within the laminate. The camera was triggered using the strain output from the incident bar. A time delay was added to account for the time taken for the pulse to travel from the strain location to the specimen. The frame rate on the camera was set at 30,000 fps, which adequately captured the failure progression in the face sheet of the specimen. The number of frames recorded by the camera was limited to 16 due to the number of CCD modules and this restricted the recording time to 500 μs. Lighting was provided by a Photogenic Powerlight 2500DR 1000 W. This light system was triggered by the camera and set to flash at 379 W with an ambient light setting of 134 W.

To verify the use of new fixture in the system, the strain uniformity in the specimen during loading was investigated. Resistance strain gauges were attached to specimens at the locations shown in Figure 2 in Section 2 ('Materials and Specimens'). Two cases were tested: uniformity between the faces, and uniformity across the face. Strain was recorded at 2.0 MHz and recorded for a total
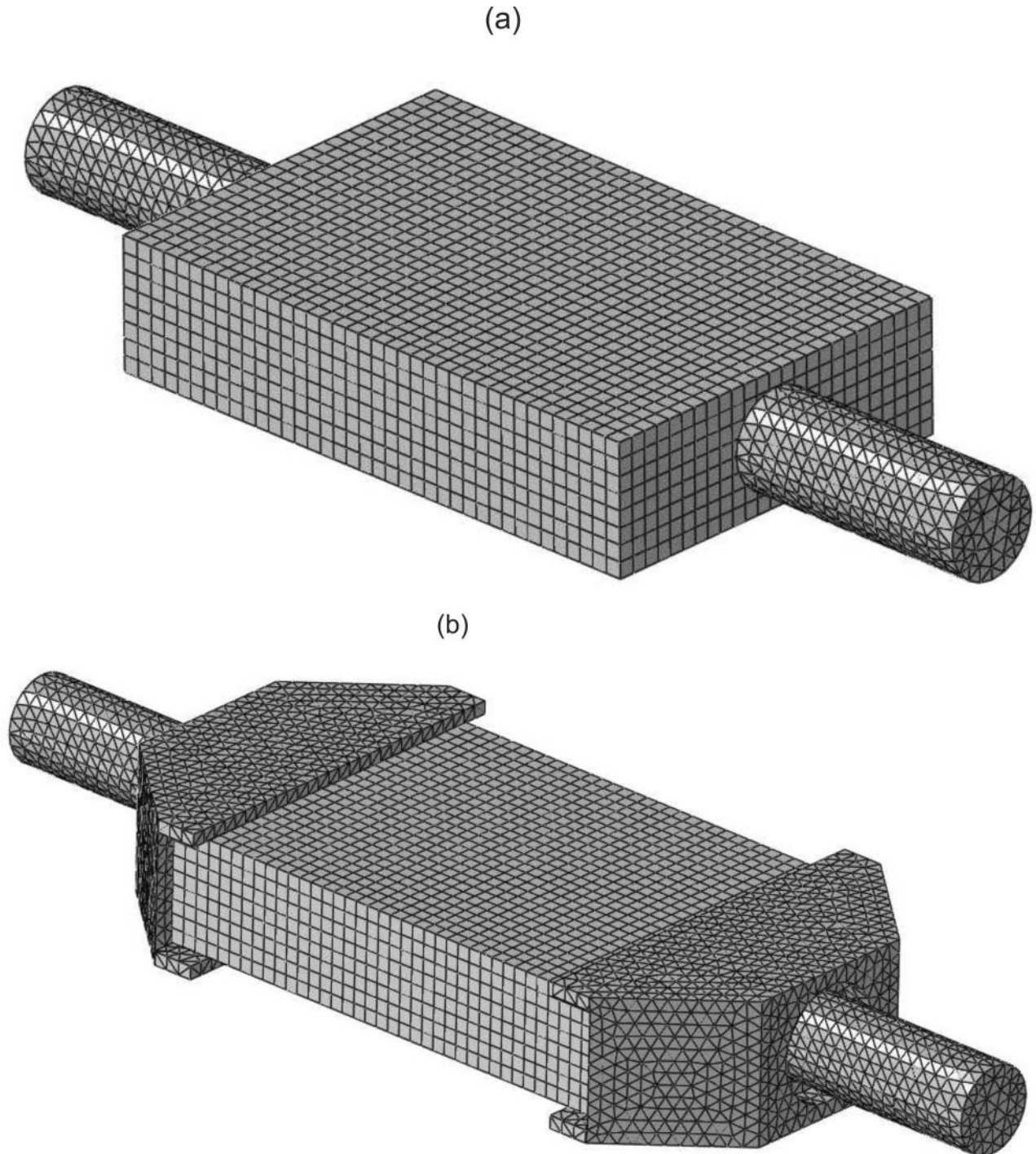
(a)

(b)

Figure 7.   Split Hopkinson Pressure Bar (SHPB) test configurations with FEA mesh: (a) without modification, (b) with new fixture.

duration of approximately 1400 μs. Impact tests were carried out at loading levels low enough to avoid failure of the specimen. The strain data shown in Figures 12a and 12b show the results of a 3.3-m/s impact and strain rate of 28.7 s^{-1}.

A difference in strain recorded between the two face sheets indicates bending in the specimen. The percentage bending (B_y) in the specimen can be calculated using Equation (5). A maximum allowable bending of 10% at a maximum applied force is specified in the static edgewise
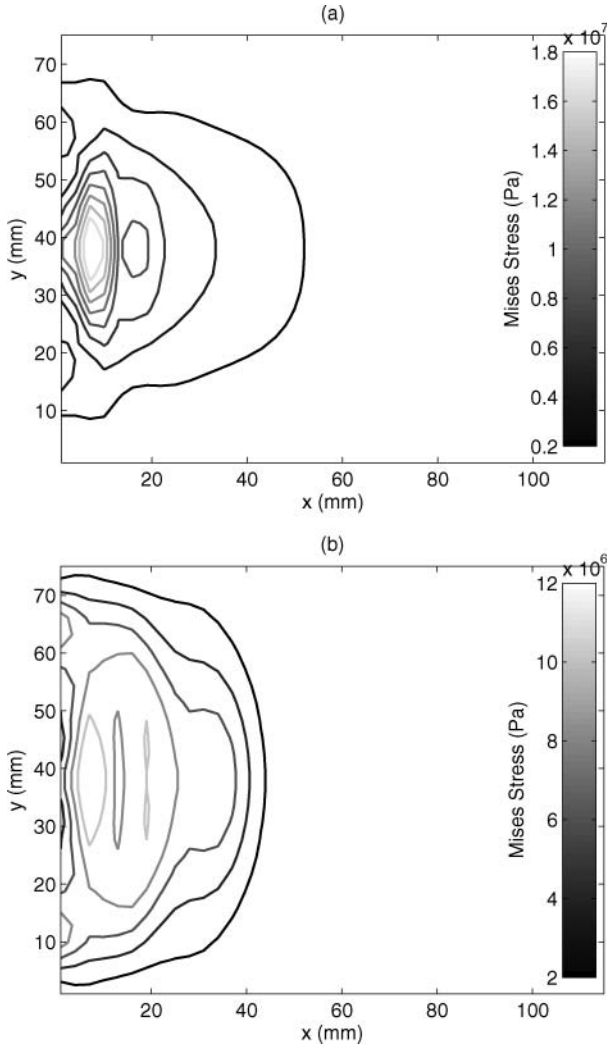
Figure 8. Progression of wave front through the sandwich structure face sheet for a 5.5-m/s impact at $t = 20$ μs (after initial impact): (a) without modification, (b) with new fixture.

Figure 9. New Split Hopkinson Pressure Bar (SHPB) fixture geometry manufactured from steel with dimensions in millimetre.

compression test standard [2]. A bending of 5.7% was calculated for the test data displayed in Figure 12a,

$$B_y = 100 \frac{\varepsilon_1 - \varepsilon_2}{\varepsilon_1 + \varepsilon_2}. \tag{5}$$

The correlation between strain channels was also quantified using the Russell Error Method [15, 20]. This method evaluates differences in phase and magnitude between transient data sets to give an overall error measure. For determining the correlation between arbitrary variables A and B, the magnitude (M_R), phase (P_R) and total comprehensive error (C_R) values are calculated respectively using Equations (6)–(9) (a_i and b_i refer to the values of independent variables for each data point and N is the total number of data points):
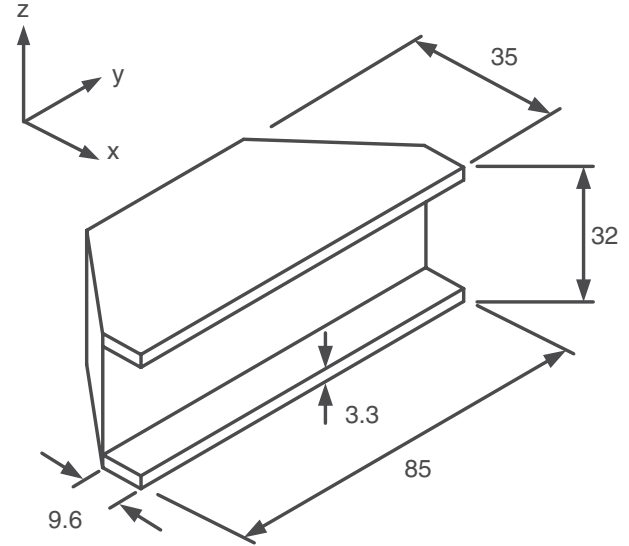
$$M_R = \sqrt{\frac{\psi_{AA}}{\psi_{BB}}} - 1, \tag{6}$$

$$P_R = \frac{1}{\pi} \cos^{-1}\left(\frac{\psi_{AB}}{\sqrt{\psi_{AA}\psi_{BB}}}\right), \tag{7}$$

$$C_R = \sqrt{M_R^2 + P_R^2}, \tag{8}$$

where

$$\psi_{AA} = \frac{\sum_i^N a_i^2}{N}, \quad \psi_{BB} = \frac{\sum_i^N b_i^2}{N}, \quad \psi_{AB} = \frac{\sum_i^N a_i b_i}{N}. \tag{9}$$

The error is classified as excellent ($C_R < 0.15$), acceptable ($0.15 < C_R < 0.28$) or poor ($C_R > 0.28$). For the distribution of load between two face sheets, the correlation between the strain profiles in Figure 12a gives a C_R value of 0.134, which is classified as excellent. For the comparison of strain profiles across the width of the face sheet given in Figure 12b, the C_R value is 0.0941, which is also considered an excellent correlation. This gives confidence that the specimens were being loaded evenly with modifications to the SHPB system.

4. Results and discussion

An experimental test program was undertaken to investigate the effect of out-of-plane compression damage on the dynamic residual strength of a thin face sheet sandwich structure. The damage tolerance investigation was carried out by first damaging the specimens using the quasi-static
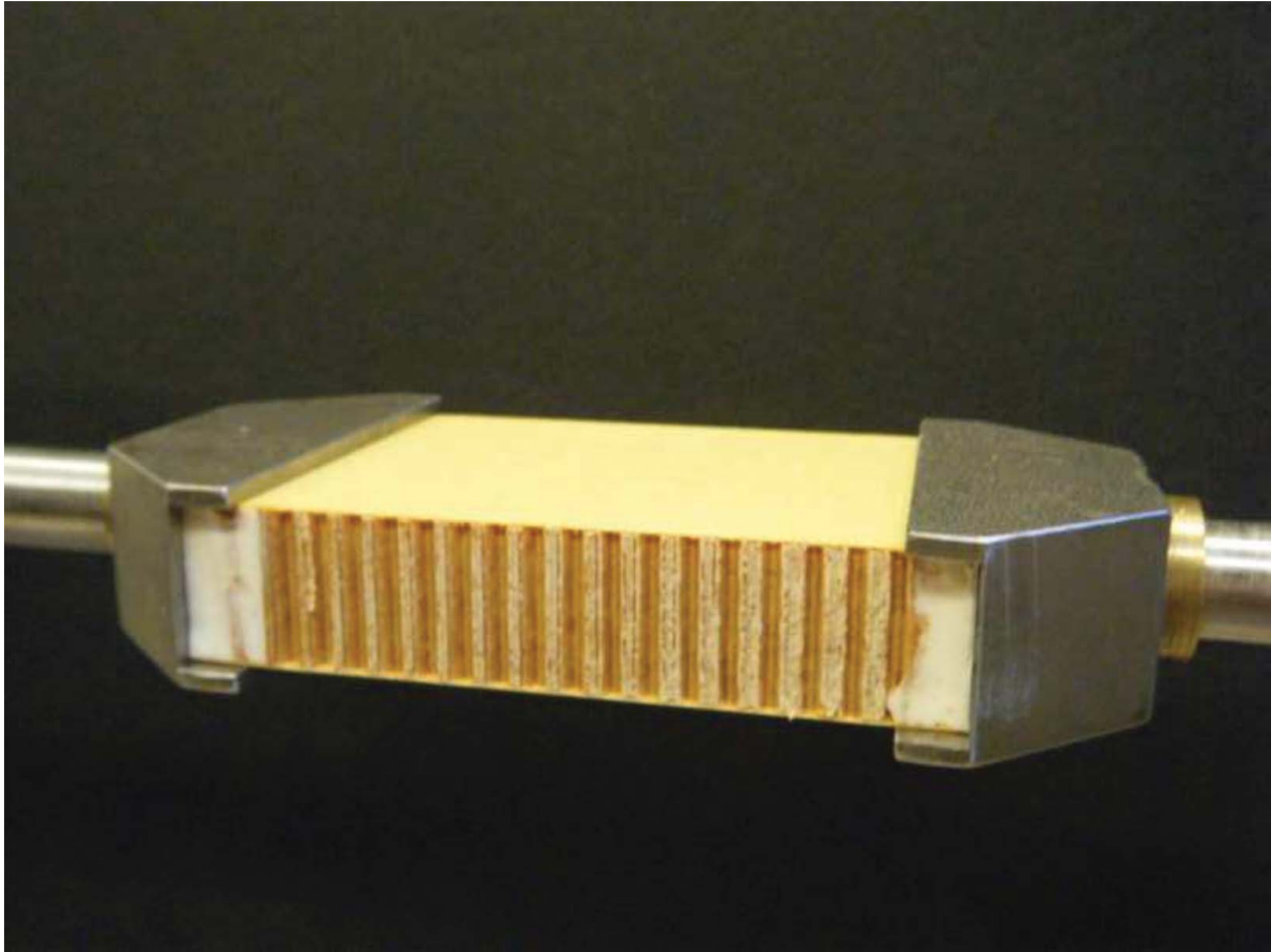
N.W. Bailey et al.

Figure 10.   Modification to Split Hopkinson Pressure Bar (SHPB) showing new fixture and attached sandwich specimen.
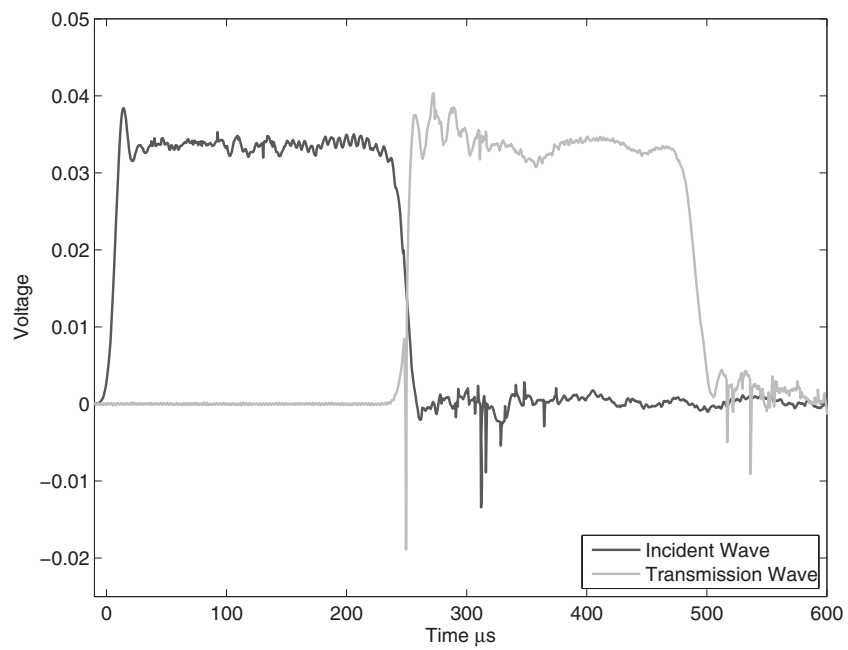

Figure 11.   Calibration graph for Split Hopkinson Pressure Bar (SHPB) showing voltage output from strain gauges.
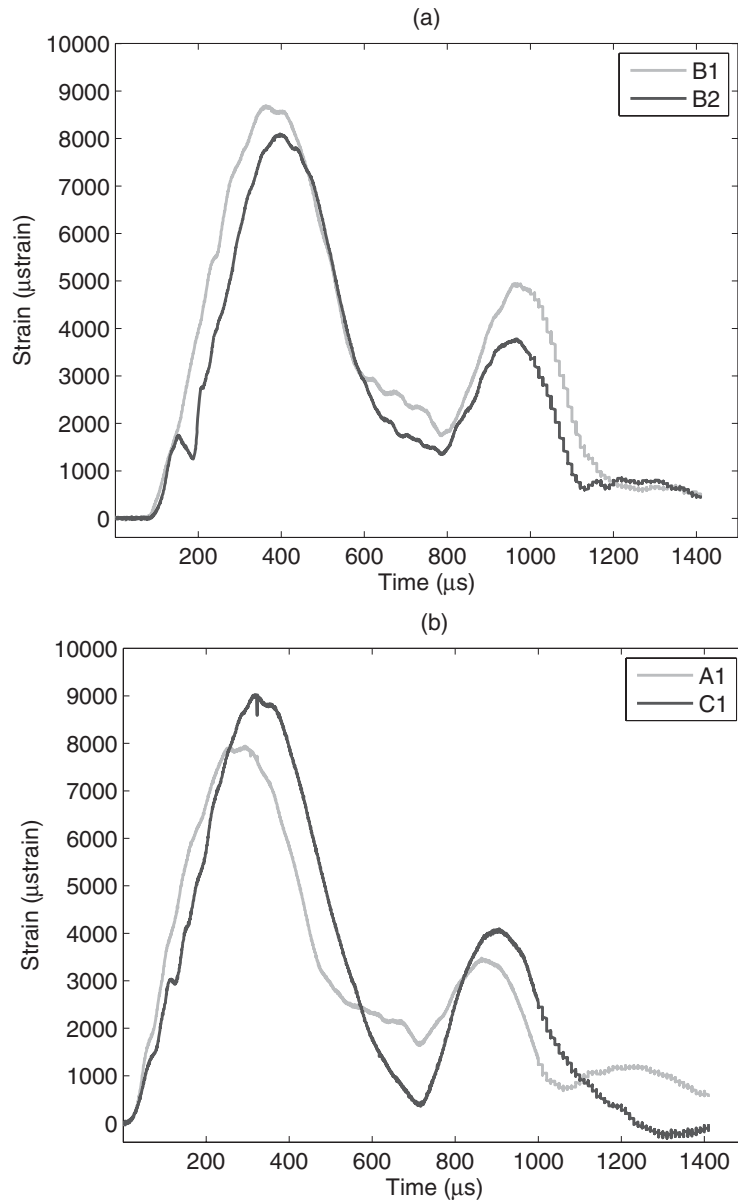
Figure 12.   Comparative strain output for a 3.3-m/s impact, (a) for gauges in the centre of each face sheet, (b) for gauges on the edges of one face sheet.

damage creation process, followed by dynamic edgewise loading at a target strain rate of 50 s^{-1}. Two specimens were tested for each damage scenario of 0.22, 0.67 and 1.7-mm residual dent depth. Time-histories of voltage data recorded at two resistance strain gauge locations in the transmission and incident bars were post-processed in Matlab. Complete SHPB results from the test of the specimen with no prior damage are shown in Figure 13. This demonstrates how the incident, transmission and reflected waves (shown in Figures 13b, 13c and Figure 13d respectively) are extracted from the raw data (Figure 13a). The data are then processed

using Equations (3) and (4) to plot stress (Figure 13e) and strain (Figure 13f).

In order to validate the SHPB method modification to test sandwich structures, strain outputs were compared by the SHPB method (strain outputs from loading bars) and the strain gauges located on the specimen. This method was used successfully by Goldberg et al. [8] to verify the modification made to test the dynamic tensile properties of carbon/epoxy composite laminates using the SHPB system. Strain results from gauges located on undamaged specimens were used for comparisons: one gauge from the
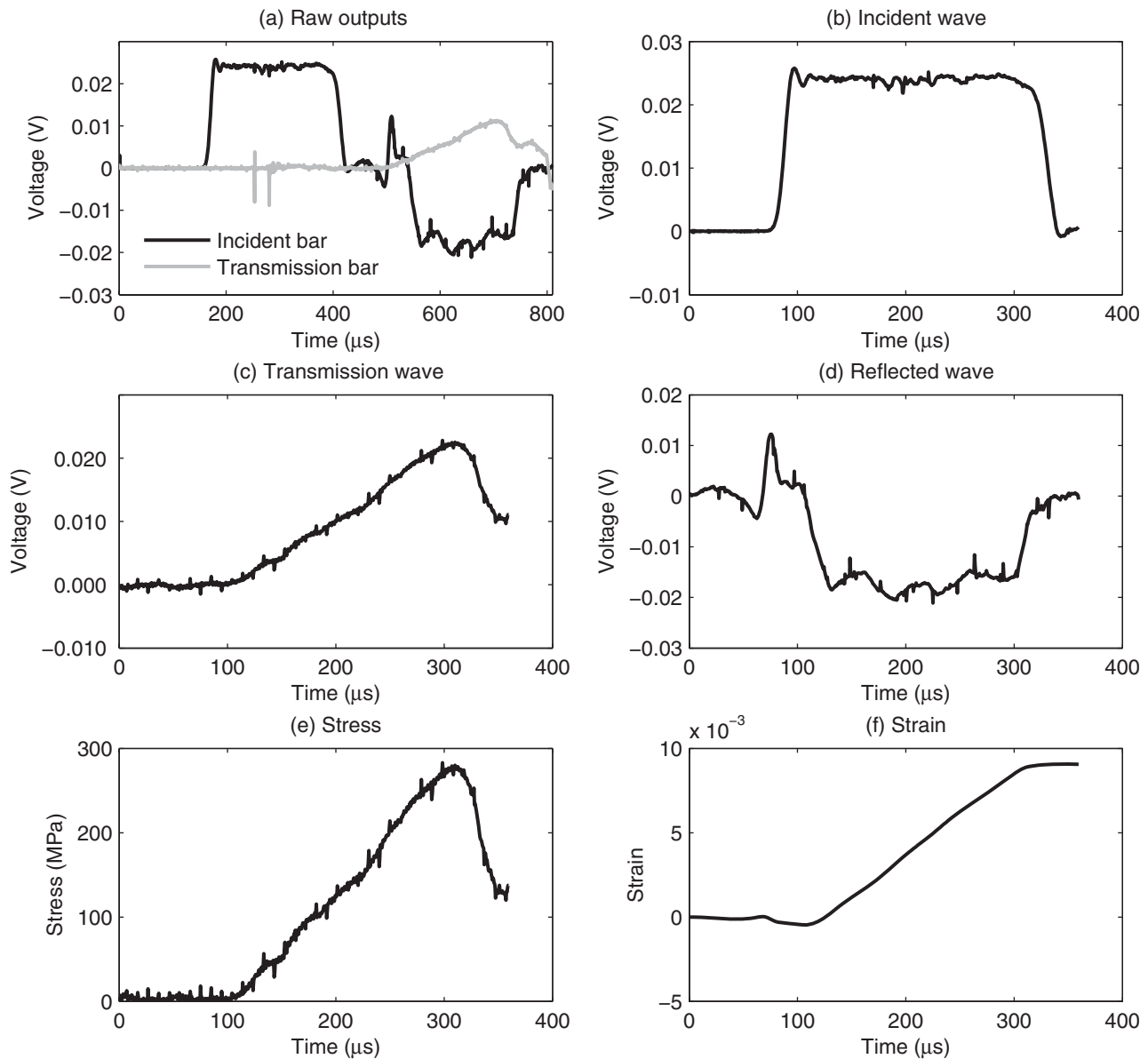
Figure 13.   Split Hopkinson Pressure Bar (SHPB) output and processing of data.

central location (gauge B1 shown in Figure 2) and another from the edge location (gauge A1 shown in Figure 2). Strain results from the gauges and the SHPB derivation are shown in Figure 14. Despite some oscillation in the data the slope of the strain profile is similar for each data set and the maximum strain values reached at the failure point are also comparable. This verifies that the calculation of strain via the SHPB method from the gauges on the incident and transmission bars is successful in producing meaningful results with the addition of new fixtures into the SHPB system.

Results for the dynamic tests were compared with previous static edgewise compression results. Static residual strength results gave an average ultimate failure stress of

235 ± 10 MPa. The Hoff and Mautner wrinkling failure approximation (Equation (1)) gives a failure stress of 250 MPa, which is 6.4% higher than the average failure stress from static edgewise compression tests. Conversely, average dynamic compressive failure occurred at 296 ± 18 MPa, which is an increase of 26% compared with the static edgewise compression and an 18% increase compared with the Hoff and Mautner approximation. This is significantly less than the 88% increase observed by Heimbs et al. [11] from tensile tests of the constituent face sheet material at the same strain rate of $50\,\mathrm{s}^{-1}$ but similar to the 25% increase in stabilised out-of-plane crush strength. During wrinkling failure the face sheet buckles locally, causing compression
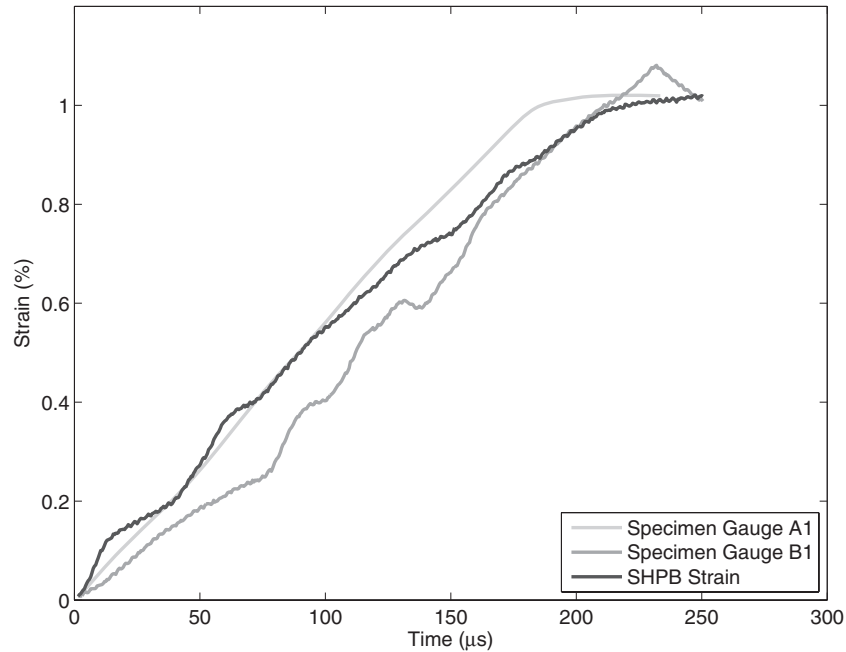
Figure 14.   Strain comparisons for Split Hopkinson Pressure Bar (SHPB) method and strain gauges on specimen.

of the core in the out-of-plane direction. Therefore, the observed rate effect may not just be a result of rate dependency of the glass-phenolic face sheet material and is possibly related to the sensitivity of the Nomex® Honeycomb to inertial effects during out-of-plane compression of the core as a result of wrinkling failure.

Final failure of the undamaged static specimens was commonly a compressive face sheet fracture across the centre of one face sheet as a result of wrinkling instability as shown in Figure 15a. Dynamic failure of an undamaged specimen shown in Figure 15b demonstrates substantial branching of the crack. Crack branching is the result of increased availability of kinetic energy due to high-impact velocities. This has been found to be a phenomenon in the dynamic failure of brittle fibre-reinforced plastics, especially under impact loading [5]. When the energy being

imparted to the specimen can no longer be dissipated by an increase in crack velocity, branching occurs, which creates more fractured surfaces for absorbing energy [6].

4.1.   *Damage tolerance*

The residual strength testing was carried out using damaged specimens with 0.22, 0.67 and 1.77-mm deep residual dents in the centre of one face sheet. An example of failure mechanisms during residual strength testing (static and dynamic) of damaged samples is shown in Figure 16. The examples show the results of dynamic impact on pre-damaged specimens with a 1.7-mm indentation. Distinctly different failure mechanisms were observed in the early stages of damaged propagation for the shown static and dynamic loading rates. In the static case, the dent depth increased with load until

Table 2.   Residual strength results summary.

| Loading type	Strain rate (s^{-1})	Residual damage (mm)	Damage energy (J)	Edgewise failure load (kN)	Edgewise compressive strength (MPa)	Standard deviation
Static	7.20e-05	0	0	17.6	235.2	10.41
Static	7.20e-05	0.22	0.11	15.1	200.8	5.15
Static	7.20e-05	0.67	0.44	12.1	161.5	7.43
Static	7.20e-05	1.7	0.98	10.2	136.7	5.03
Dynamic	51.9	0	0	22.2	296.1	18.3
Dynamic	46.1	0.22	0.11	16.3	217.3	1.77
Dynamic	44.7	0.67	0.44	13.7	182.5	3.54
Dynamic	45.1	1.7	0.98	13	173.1	0.57
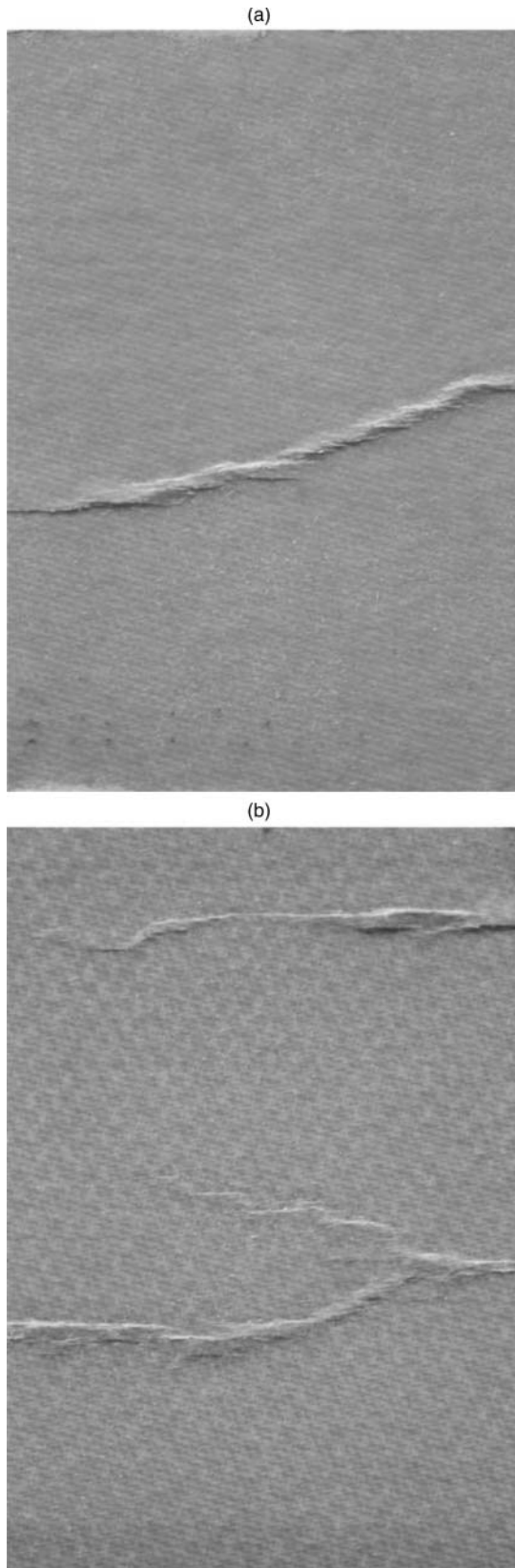
Figure 15.   Post-failure photos of edgewise compression failure: (a) static (strain rate $= 7.2 \times 10^{-5}$ s^{-1}), (b) dynamic (strain rate $\approx$ 50 s^{-1}).

the crack slowly moved out from the central damage region. At the final failure point, rapid propagation of the crack occurred resulting in complete failure of the face sheet across the width of the specimen. In the case of dynamic failure (Figure 16) the dent region grew in depth and also in width as load increased. Fracture of the specimen initiated at the edge of this buckled region with a final crack propagating to the edge of the specimen. Complete failure of the specimen took 22 μs in the dynamic case compared with 24 ms in the static case. The increased indentation of the core in the pre-existing damage region during the dynamic loading event causes rapid compression of core in the out-of-plane direction before the final fracture of the face sheet. Therefore, the effect of dynamic loading on pre-damaged specimens could also be related to the sensitivity of the honeycomb core to inertial effects.

A summary of the static and dynamic residual strength results are given in Table 2 showing the significance of loading rate on damaged specimens. Failure load is determined from the force data profiles where the catastrophic failure of the face sheet causes a sudden drop in the applied load. The standard deviation values given in Table 2 indicate that there is more variability in the edgewise compression strength for specimens with no damage regardless of whether the loading is static or dynamic. Damaged specimens provide an initiation point in the damaged region from where a crack will most likely propagate. Without prior damage in the specimen, compression failure is initiated at the edge of the face sheet and attributed to local instability of the face sheet commonly known as wrinkling. In this case failure occurs as one rapid event in both static and dynamic loading of undamaged specimens. Therefore, without a specific initiation point for the compressive failure to propagate from, the variability in compressive residual strength test data increases.

The dynamic residual strength results are summarised in Figure 17, including a comparison to the static results. Error bars for each test case showing ± 1 standard deviation quantify the variability. The dynamic damage tolerance curve in Figure 17 is offset above the static curve, meaning that for all levels of prior damage the residual compressive strength is higher for dynamic loading compared with static loading. The reduction in dynamic compressive strength for damaged specimens is sensitive to even small damage, illustrated by a 27% decrease in compressive strength on average between undamaged specimens and those with a 0.22-mm residual dent; static residual tests of specimens with equivalent damage resulted in a 15% reduction in compressive strength. A plateau region is evident in each of the damage tolerance curves shown in Figure 17 where the residual strength levels off between dent depths of 0.66 and 1.7 mm. This region corresponds with the transition point in the damage-creation phase, where the face sheet is penetrated beyond a dent depth of approximately 1.2 mm (displaced depth of 2.5 mm).
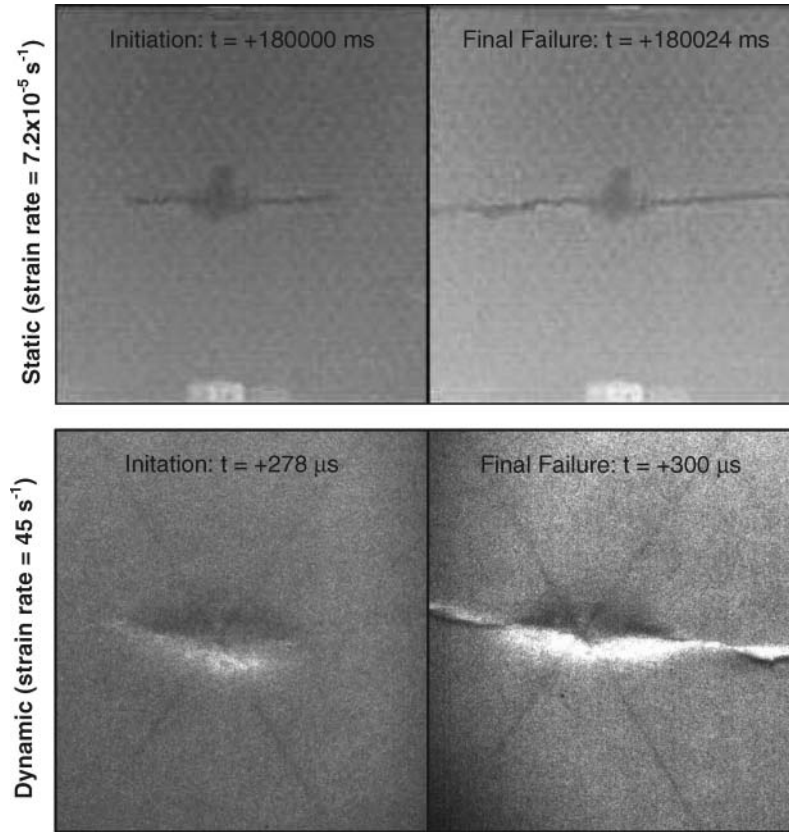
Figure 16. High-speed video capture of static and dynamic edgewise compression failure mechanisms for sandwich specimens with prior damage of a 1.7-mm dent (time values refer to time).
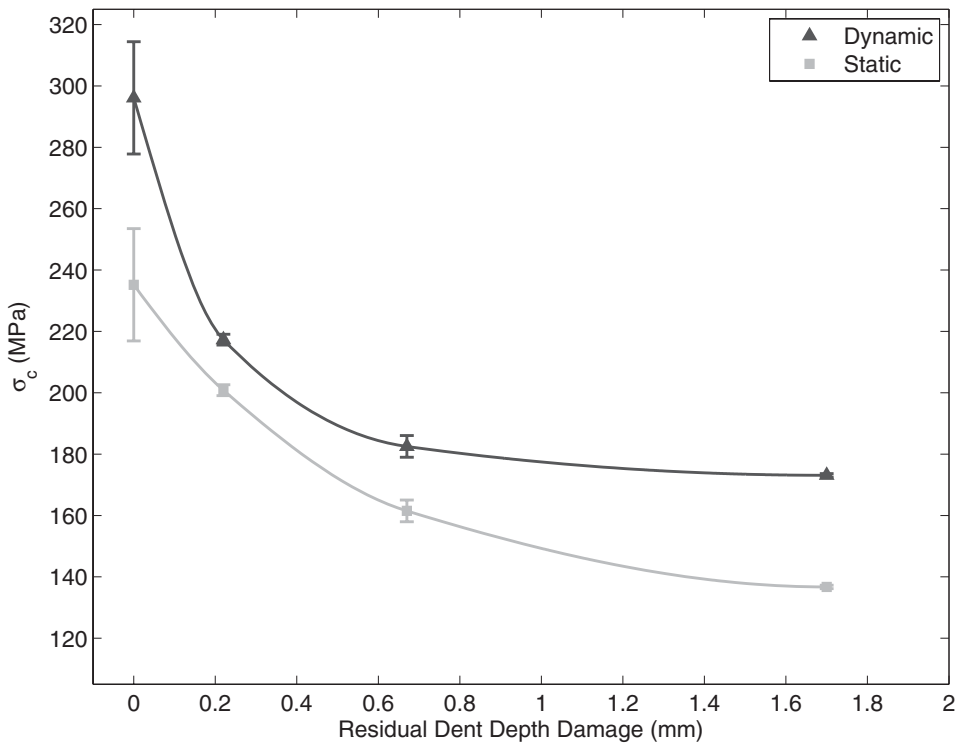

Figure 17. Residual strength profile for static (strain rate $= 7.2 \times 10^{-5}$ s^{-1}) and dynamic (strain rate ≈ 50 s^{-1}) edgewise compression tests.

5. Conclusions

A test method has been developed for dynamic edge-wise compression loading of sandwich structures based on SHPB methodology. The new test method has successfully enabled dynamic edgewise compression characterisation of glass-phenolic Nomex® honeycomb sandwich structures at a strain rate of approximately 50 s^{-1}. Calibration and verification tests demonstrated that the addition of steel fixtures to incorporate a sandwich structure specimen into the SHPB system achieved acceptable uniformity of the specimen strain fields.

Comparisons were made between the dynamic tests and equivalent static edgewise test results for undamaged specimens. Results for dynamic residual strength showed an average increase of 26% in compression strength compared to equivalent static tests. Significant branching of cracks was observed during dynamic failure of the face sheet.

In the case of specimens with pre-existing damage, a higher dynamic residual strength was recorded for all cases of indentation damage compared with static residual strength. Residual strength tests showed increased indentation into the core during dynamic failure that was not observed in static tests. Even for low levels of indentation damage (0.22-mm dent depth) there was a 27% reduction in residual dynamic compressive strength compared with a 15% reduction in residual static compressive strength for equivalent prior damage.

Characterisation of sandwich structures solely using static test methods may therefore not be definitive in predicting the force response and mechanisms of failure when subjected to dynamic loads. This study illustrates important phenomena in the edgewise compressive response of sandwich structures under dynamic loading that require consideration in the design of aircraft components utilising sandwich structures.

Acknowledgements

References

[1] ASTM International, *ASTM, Standard Test Method for Facing Properties of Sandwich Constructions by Long Beam Flexure, in* D7249/D7249M – 06, ASTM International, West Conshohocken, PA, 2006.

[2] ASTM International, *ASTM, Standard Test Method for Edgewise Compressive Strength of Sandwich Construc-tions, in* C 364/C 364M – 07, ASTM International, West Conshohocken, PA, 2007.

[3] N. Bailey, M. Battley, and M. Zhou, *Dynamic damage tolerance for aircraft sandwich structures: experiments and modeling*, Proceedings of the 52nd Structures Conference of American Institute of Aeronautics and Astronautics, Denver, CO, 2011.

[4] S. Barré, T. Chotard, and M.L. Benzeggagh, *Comparative study of strain rate effects on mechanical properties of glass fibre-reinforced thermoset matrix composite*, Composites A: Appl. Sci. Manuf. 27 (1996), pp. 1169–1181.

[5] I. Daniel, E. Gdoutos, and Y. Rajapakse, *Major Accomplishments in Composite Materials and Sandwich Structures: An Anthology of ONR Sponsored Research*, Springer, New York, 2009.

[6] V. Evora, N. Jain, and Shukla, *Static and dynamic fracture toughness and crack propagation in nanocomposites*, Proceedings of the 11th Conference on Fracture, Turin, Italy, 2005.

[7] Federal Aviation Administration, *FAA, PART 25 – Airworthiness Standards: Transport Category Airplanes, Subpart C – Structure, Emergency Landing Conditions, in Federal Aviation Regulations*, D.o.T., Federal Aviation Administration, Washington, DC, 2012.

[8] A. Gilat, R.K. Goldberg, and G.D. Roberts, *Experimental study of strain-rate-dependent behavior of carbon/epoxy composite*, Compos. Sci. Technol. 62 (2002), pp. 1469–1476.

[9] P.R. Hampson and M. Moatamedi, *A review of composite structures subjected to dynamic loading*, Int. J. Crashworthiness 12 (2007), pp. 411–428.

[10] J.J. Harrigan, S.R. Reid, and C. Peng, *Inertia effects in impact energy absorbing materials and structures*, Inter. J. Impact Eng. 22 (1999), pp. 955–979.

[11] S. Heimbs, P. Middendrof, C. Hampf, F. Hahnel, and K. Wolf, *Numerical simulation of aircraft interior components under crash loads*, Int. J. Crashworthiness 13 (2008) pp. 511–521.

[12] S. Heimbs, S. Schmeer, P. Middendrof, and M. Maier, *Strain rate effects in phenolic composites and phenolic-impregnated honeycomb structures*, Compos. Sci. Technol. 67 (2007), pp. 2827–2837.

[13] Hexweb, *Hexweb Honeycomb Sandwich Design Technology*, Hexcel Composites, Cambridge, 2000.

[14] N.J. Hoff and S.E. Mautner, *The buckling of sandwich type panels*, J. Aeronaut. Sci. 12 (1945, July), p. 285.

[15] J. LeBlanc and A. Shukla, *Dynamic response and damage evolution in composite materials subjected to underwater explosive loading: An experimental and computational study*, Compos. Struct. 92 (2010), pp. 2421–2430.

[16] R. Ley, W. Lin, and U. Mbanefo, *Facesheet Wrinkling in Sandwich Structures*, NASA Langley Research Center, Hampton, VA, 1999.

[17] U.S. Lindholm, *Some experiments with the split Hopkinson Pressure Bar*, J. Mech. Phys. Solids 12 (1964), p. 18.

[18] H. Mahfuz, W.A. Mamun, A. Haque, S. Turner, H. Mohamed, and S. Jeelani, *An innovative technique for measuring the high strain rate response of sandwich composites*, Compos. Struct. 50 (2000), pp. 279–285.

[19] S.W. Park, M. Zhou, and D.R. Veazie, *Time-resolved impact response and damage of fiber-reinforced composite laminates*, J. Compos. Mater. 34 (2000), pp. 879–904.

[20] H. Sarin, M. Kokkolaras, G. Hulbert, P. Papalambros, S. Barbat, and R.J. Yang, *Comparing time histories for validation of simulation models: error measures and*

metrics, J. Dyn. Syst., Meas. Control 132 (2010), pp. 061401-1–061401-10.

[21] A. Shipsha and D. Zenkert, *Compression-after-impact strength of sandwich panels with core crushing damage*, Appl. Compos. Mater. 12 (2005), pp. 149–164.

[22] R.L. Sierakowski and S.K. Chaturvedi, *Dynamic Loading and Characterization of Fiber-Reinforced Composites*, John Wiley, New York, 2007.

[23] D.D. Symons, *Characterisation of indentation damage in 0/90 lay-up T300/914 CFRP*, Compos. Sci. Technol. 60 (2000), pp. 391–401.

[24] J. Tomblin, T. Lacy, B. Smith, and A. Hooper, *Review of Damage Tolerance for Composite Sandwich Airframe Struc-*

tures, US Department of Transportation, Federal Aviation Administration, 1999.

[25] T.K. Tsotsis and S.M. Lee, *Characterization of localized failure modes in honeycomb sandwich panels using indentation*, in *Composite Materials: Testing and Design* Vol. 12 (ASTM STP 1274), ASTM International, West Conshohocken, PA, 1996, p. 26.

[26] D. Zenkert, *An Introduction to Sandwich Construction*, Wiley-Blackwell, Hoboken, NJ, 1995.

[27] H. Zhao and G. Gary, *Crushing behaviour of aluminium honeycombs under impact loading*, Int. J. Impact Eng. 21 (1998), pp. 827–836.